

D-A088 080

PENNSYLVANIA STATE UNIV UNIVERSITY PARK DEPT OF MECH--ETC F/8 21/9.2
TRANSIENT IGNITION MECHANISMS OF CONFINED SOLID PROPELLANTS UND--ETC(111)
AUG 80 K K KUO, M KUMAR, A K KULKARNI N00014-79-C-0762

NL

UNCLASSIFIED

1 of 1

25

000000

000000

END
DATE
FILMED
9-80
DTIC

LEVEL II

12



AD A088080

**TRANSIENT IGNITION MECHANISMS OF
CONFINED SOLID PROPELLANTS UNDER
RAPID PRESSURIZATION**

SUMMARY REPORT

Sponsored by
Office of Naval Research
Power Program
Arlington, Virginia
Contract No. N00014-79-C-0762

Prepared by
K. K. Kuo, M. Kumar and A. K. Kulkarni

August, 1980

SELECTED
AUG 18 1980
C

This document has been approved
for public release and sale; its
distribution is unlimited.

THE PENNSYLVANIA STATE UNIVERSITY
College of Engineering
Department of Mechanical Engineering
University Park, Pennsylvania

80 8 15 025

SECURITY CLASSIFICATION OF THIS PAGE (When Data Entered)

REPORT DOCUMENTATION PAGE		READ INSTRUCTIONS BEFORE COMPLETING FORM
1. REPORT NUMBER	2. GOVT ACCESSION NO. A088 080	3. RECIPIENT'S CATALOG NUMBER 7
4. TITLE (and Subtitle) 6 Transient Ignition Mechanisms of Confined Solid Propellants under Rapid Pressurization		5. TYPE OF REPORT & PERIOD COVERED Summary August 1, 1979 - July 31, 1980
7. AUTHOR(s) 10 K. K. Kuo, M. Kumar, A. K. Kulkarni		6. PERFORMING ORG. REPORT NUMBER 1 Aug 79-31 Jul 80
		8. CONTRACT OR GRANT NUMBER(s) 15 N00014-79-C-0762
9. PERFORMING ORGANIZATION NAME AND ADDRESS Department of Mechanical Engineering The Pennsylvania State University University Park, PA 16802		10. PROGRAM ELEMENT, PROJECT, TASK AREA & WORK UNIT NUMBERS
11. CONTROLLING OFFICE NAME AND ADDRESS Office of Naval Research Power Program Arlington, Virginia 22217	11 6	12. REPORT DATE August 1980
14. MONITORING AGENCY NAME & ADDRESS (if different from Controlling Office) 12 58		13. NUMBER OF PAGES 57
		15. SECURITY CLASS. (of this report) Unclassified
		15a. DECLASSIFICATION/DOWNGRADING SCHEDULE
16. DISTRIBUTION STATEMENT (of this Report) Approved for public release, distribution unlimited.		
17. DISTRIBUTION STATEMENT (of the abstract entered in Block 20, if different from Report)		
18. SUPPLEMENTARY NOTES		
19. KEY WORDS (Continue on reverse side if necessary and identify by block number) Ignition of solid propellants, theoretical modelling, propellant cracks, flame propagation, combustion/solid mechanics interaction, deflagration-to- detonation transition.		
20. ABSTRACT (Continue on reverse side if necessary and identify by block number) see next page		

DD FORM 1473 1 JAN 73 EDITION OF 1 NOV 65 IS OBSOLETE

SECURITY CLASSIFICATION OF THIS PAGE (When Data Entered)

401 929

JP

ABSTRACT

A comprehensive theoretical model was formulated to study the transient ignition mechanisms of solid propellants under rapidly varying pressure conditions. The model considers a two-dimensional geometry to describe the ignition of a heterogeneous propellant. The rate of pressurization has been included in the energy equation to simulate rocket motor ignition conditions. The model does not make any *a priori* assumption of solid-phase, heterogeneous, or gas-phase ignition mechanism. Chemical reactions are considered in the gas phase, at the interface as well as in the subsurface. The most up-to-date chemical kinetics information is included in the model. A generalized ignition criterion has been proposed which allows ignition to occur at any site.

Development of the theoretical model was preceded by an extensive review of the literature on solid-propellant ignition to establish the state-of-the-art. Various ignition theories, experimental measurements, and ignition criteria were critically examined. Major technological gaps in solid-propellant ignition study were identified, and areas for future research were recommended.

A study was conducted to investigate flame-spreading and combustion processes in narrow propellant cracks. Experimental results show that when the crack-gap width is very small (~450 μm), several partial closures of the crack gap occur due to the propellant deformation caused by strong interaction between combustion and solid mechanics. Results from the theoretical study of the effect of propellant deformation on ignition and combustion processes in propellant cracks indicate that the effect of propellant deformation is quite important for small gap widths and high chamber pressure conditions. Calculated results also show that gap closures may generate substantial local pressure peaks.

The effects of pressurization rate, crack-gap width, crack length, and propellant type on ignition and flame-spreading processes in isolated AP-based solid propellant cracks were studied experimentally. It was observed that hot gases precede the ignition front, and that the maximum pressure in the crack cavity may significantly exceed the pressure in the chamber. The results of parametric study indicate that as the pressurization rate or burning rate of the propellant is increased, the time required for the ignition front to reach the crack tip decreases, and the maximum velocity of the ignition front increases. Maximum pressure in the crack increases with an increase in burning rate or crack length, but decreases with an increase in gap width.

Accession For		<input checked="" type="checkbox"/>
NTIS	GRA&I	
DDC TAB		<input type="checkbox"/>
Unannounced		
Justification _____		
By _____		
Distribution/_____		
Availability Codes		
Dist	Avail and/or special	
A		

TRANSIENT IGNITION MECHANISMS OF
CONFINED SOLID PROPELLANTS UNDER
RAPID PRESSURIZATION

SUMMARY REPORT

Sponsored by

Office of Naval Research
Power Program
Arlington, Virginia

Contract No. N00014-79-C-0762

Prepared by

Kenneth K. Kuo, Telephone (814) 865-6741
Mridul Kumar, Telephone (814) 863-0359
Anil K. Kulkarni, Telephone (814) 865-3340

Department of Mechanical Engineering
The Pennsylvania State University
University Park, PA 16802

Reproduction in whole or in part is permitted for
any purpose of the United States Government.

Approved for public release, distribution unlimited.

ACKNOWLEDGEMENTS

This research has been sponsored by the Power Program of the Office of Naval Research, Arlington, Virginia, under the Contract No. N00014-79-C-0762. Dr. Richard S. Miller served as the technical monitor and program manager for this contract. His support of this research investigation is greatly appreciated.

The assistance of Mr. S. M. Kovacic and Mr. J. E. Wills in the experimental part of this study is acknowledged. We would also like to thank Mrs. Doreen Packer for typing this report.

TABLE OF CONTENTS

ACKNOWLEDGEMENTS.....	iv
LIST OF FIGURES AND TABLES	vi
I. INTRODUCTION	1
II. LITERATURE SURVEY	2
III. THEORETICAL WORK	5
3.1 Development of a Comprehensive Ignition Model	5
3.1.1 Introduction	5
3.1.2 Physical Description of the Ignition Model	7
3.1.3 Governing Equations	9
3.1.4 Initial and Boundary Conditions	11
3.1.5 Chemical Kinetics Information	15
3.2 Investigation of Combustion/Solid Mechanics Interaction in Narrow Cracks	22
IV. EXPERIMENTAL WORK	30
4.1 Development of a New Igniter System	30
4.2 Improvements in Data Acquisition System	30
4.3 Experimental Observations of Flame Spreading and Combustion in Narrow Cracks	31
V. NOMENCLATURE	37
VI. REFERENCES.....	39
APPENDIX I---Abstract of "Review of Solid Propellant Ignition Studies"	41
APPENDIX II--Abstract of "Combustion-Structural Interaction in A Viscoelastic Material"	42
APPENDIX III-Abstract of "Effect of Propellant Deformation on Ignition and Combustion Processes in Solid Propellant Cracks"	43
APPENDIX IV--Abstract of "Gas Penetration, Flame Propagation, and Combustion Processes in Solid Propellant Cracks"	45

LIST OF FIGURES AND TABLES

<u>Figure</u>	<u>Caption</u>	<u>Page</u>
1	Physical Processes Involved in Solid Propellant Ignition	6
2	Schematic Diagram of a Heterogeneous Solid Propellant	8
3	Modified Cross-sectional View of a Statistically Averaged Element Considered in the Ignition Model. . .	8
4	General Layout of Coupled Combustion/Solid Mechanics Computer Program	24
5	Finite Element Grid and Finite Difference Nodes	25
6	Calculated Pressure Distribution at Various Times during Crack-Gap Closure (Case 1).	27
7	Calculated Pressure Distribution at Various Times during Crack-Gap Closure (Case 2).	28
8	Schematic Diagram of Crack Combustion and Igniter System	32
9	Propellant Sample Used for Detailed Observation of Flame Front.	33
10	Block Diagram of Data Acquisition System	34
11	A Sequence of Photographs Showing Crack-Gap Closures .	35
 <u>Table</u>		
1	Initial and Boundary Conditions for Gas Phase.	11

I. INTRODUCTION

This report summarizes the progress made during the period August 1, 1979 to July 31, 1980 under the project entitled "Transient Ignition Mechanisms of Confined Solid Propellants under Rapid Pressurization" (Contract No. N00014-79-C-0762).

The overall objective of this investigation is to achieve a better understanding of the ignition process of a solid propellant under rapidly varying pressure conditions. These fundamental studies are expected to help in the design of solid rocket motors and in reducing the hazards caused by convective burning and deflagration-to-detonation transition processes. The report covers three major areas: 1) literature survey; 2) theoretical work; and 3) experimental work. These topics are discussed in detail in Sections II, III and IV.

The following publications represent a part of the work performed under the contract.

- (1) "Review of Solid Propellant Studies," AIAA Paper No. 80-1210, AIAA/SAE/ASME 16th Joint Propulsion Conference, June 30 - July 2, 1980, Hartford, CT (by A. K. Kulkarni, M. Kumar, and K. K. Kuo).
- (2) "Gas Penetration, Flame Propagation, and Combustion Processes in Solid Propellant Cracks," AIAA Paper No. 80-1206, AIAA/SAE/ASME 16th Joint Propulsion Conference, June 30 - July 2, 1980, Hartford, CT (by M. Kumar, S. M. Kovacic, and K. K. Kuo).
- (3) "Combustion - Structural Interaction in a Viscoelastic Material," Symposium on Computational Methods in Nonlinear Structural and Solid Mechanics, October 6-8, 1980, Washington, DC (by T. Y. Chang, J. P. Chang, M. Kumar, and K. K. Kuo).
- (4) "Effect of Propellant Deformation on Ignition and Combustion Processes in Solid Propellant Cracks," to be presented at the JANNAF Propulsion Systems Hazards Subcommittee Meeting, October 27-31, 1980, Naval Postgraduate School, Monterey, CA (by M. Kumar and K. K. Kuo).

II. LITERATURE SURVEY

An excellent review of solid propellant ignition research was conducted fourteen years ago by Price et al.¹ (1966). Numerous ignition studies resulting in significant progress have been made in the interim. To fully utilize past experience and knowledge, an extensive literature survey² was made. This review was presented at the AIAA/SAE/ASME 16th Propulsion Conference in Hartford, Connecticut, on June 30 - July 2, 1980; the abstract of this paper is given in Appendix

I. Specific objectives of the review were:

- (1) to establish the state-of-the-art in the study of solid-propellant ignition;
- (2) to identify technological gaps and contradictions in the existing literature;
- (3) to facilitate development of a comprehensive ignition theory;
and
- (4) to incorporate merits of past experimental techniques into the current test program.

The review consists of an easy-to-read tabular summary of recent important works in the area of solid propellant ignition, giving basic assumptions, theoretical formulation, apparatus description, range of experimental parameters, ignition criteria, important results, and conclusions. Critical comments on each work are also listed. The tabular form is designed to facilitate comparison between various studies and to provide a quick reference.

In general, the ignition theories can be classified into three major groups. Solid-phase ignition theories emphasize the heat deposition rate in the solid; the ignition criterion is usually based upon the attainment of a critical temperature in the solid phase. Gas-phase ignition theories consider the controlling

mechanism to be the chemical reaction between vaporized fuel species and oxidizer gases; the ignition criterion is usually based upon the rate of change of the gas-phase temperature distribution. Heterogeneous ignition theories propose the controlling mechanism to be the reaction between the solid-phase fuel and ambient oxidizer at the interface; the ignition criterion is usually based upon the attainment of a critical surface temperature or a critical rate of increase of surface temperature.

Based upon study of over 100 investigations, various important aspects are discussed in the review in order to present an overall view of solid propellant ignition studies. These aspects include means of achieving ignition, description of the ignition process, governing equations and interfacial conditions (together with the physical meaning of each term), effects of various ambient and propellant parameters on ignition delay, difficulties encountered in theoretical and experimental investigations, and recommendations for future research.

As a result of this review, it was determined that some of the major technological gaps in the theory of solid propellant ignition are a) determination of the controlling mechanism at various stages of ignition, b) selection of a proper ignition criterion, c) detailed specification of chemical kinetics, and d) the heterogeneous nature of the propellant. Some of the technological gaps in the experimental area are a) realistic simulation of an actual ignition process in the laboratory, b) highly transient nature of the ignition process and the smallness of the region of interest (making data acquisition very difficult), c) the experimental definition of the instant of ignition, and d) lack of broad data base.

It is concluded that although the foundation for solid propellant ignition research is laid, it is as yet far from complete. Additional efforts are needed in the areas of a) study of the ignition process under transient conditions,

such as inclusion of pressurization rate, $\frac{dp}{dt}$, in experiments and theory (to simulate actual ignition processes in rocket motors), b) detailed consideration of chemical kinetics in theoretical models, c) consideration of heterogeneous propellants using 2-D or 3-D models, d) use of advanced instrumentation in conducting experiments on ignition, and e) establishment of a broader data base.

III. THEORETICAL WORK

The theoretical work was divided into two parts: 1) development of a comprehensive ignition model; and 2) investigation of combustion/solid mechanics interaction in narrow cracks.

3.1 Development of a Comprehensive Ignition Model

3.1.1 Introduction

Ignition of a solid propellant is a complex physicochemical phenomenon which involves various processes such as heat transfer, fluid mechanics, phase change, mass diffusion of chemical species, and chemical kinetics. Figure 1 shows typical processes involved in ignition of a heterogeneous propellant. As discussed in the review paper,² the theoretical modeling of the ignition process is complicated by such factors as the heterogeneous nature of the propellant (and the overall ignition process), specifications of chemical kinetics, determination of the controlling mechanism of the ignition process, and selection of an appropriate ignition criterion. In existing models, a number of simplifying assumptions have been made for mathematical tractability.

Keeping in mind the difficulties mentioned above, as well as the need to explain the actual ignition event adequately, a comprehensive ignition model, expected to be the most complete to date, was formulated. Highlights of this model are:

1. 2-D geometry, allowing description of a heterogeneous propellant. Thus far, only Kumar and Hermance³ have used a 2-D ignition model.
2. Inclusion of a pressurization (dp/dt) term in the governing equation for the gases surrounding the propellant to simulate actual rocket motor ignition conditions. Up to now, the only ignition model which has considered the pressurization effect is that proposed by Kumar and Kuo⁴ for 1-D geometry.

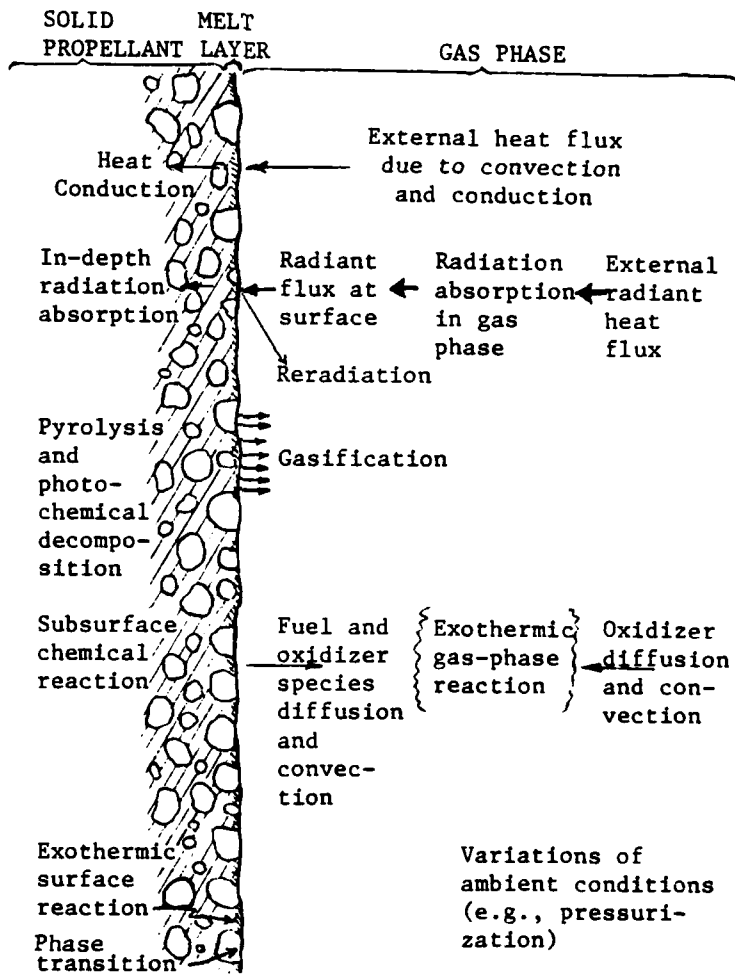


Fig. 1 Physical Processes Involved in Solid Propellant Ignition

3. No a priori assumption of a solid-phase, heterogeneous, or gas-phase reaction mechanism was made to control the ignition event. Except for the unified ignition theory of Bradley,⁵ for which very limited results were obtained, this approach is unlike that of any other previously proposed model. The current model allows chemical reactions in all regions, including the gas phase, interfaces, and subsurface.
4. A flexible "multiple" ignition criterion has been proposed to allow ignition to occur at any site, i.e., in the gas phase, at the interface, or in the solid phase.
5. Detailed chemical kinetics information was considered in development of the model.

3.1.2 Physical Description of the Ignition Model

To model the ignition of a heterogeneous propellant, one must first examine the nature of the propellant. Figure 2 shows typical side cross-sectional and top views of a composite propellant. Oxidizer particles of random size (within a certain range) are distributed in a fuel binder. For a mathematical simulation of this type of structure, a statistical size distribution of oxidizer particles is estimated. From this calculation, the radius R_1 of the oxidizer particle and the radius R_2 of the fuel binder for a typical element of the propellant are determined.

A modified cross-sectional view of a statistically averaged element, suitable for mathematical modeling, is shown in Figure 3. A cylindrical coordinate system (r,z) is selected in which initially the r axis runs along the surface, starting from the center of the oxidizer particle (which is assumed to be hemispherical at $t=0$). The axis is perpendicular to the initially planar interface and positive in the surrounding gas phase. An external radiation flux, incident upon the interface (see also Figure 1), is partly absorbed and partly reflected at the

PHYSICAL MODEL

Side Cross-sectional View

Top View

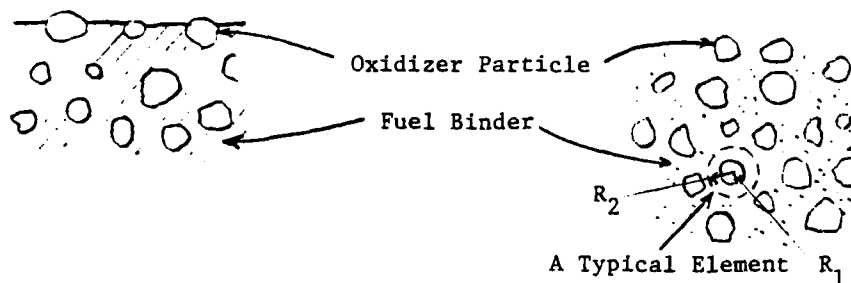


Fig. 2 Schematic Diagram of a Heterogeneous Solid Propellant

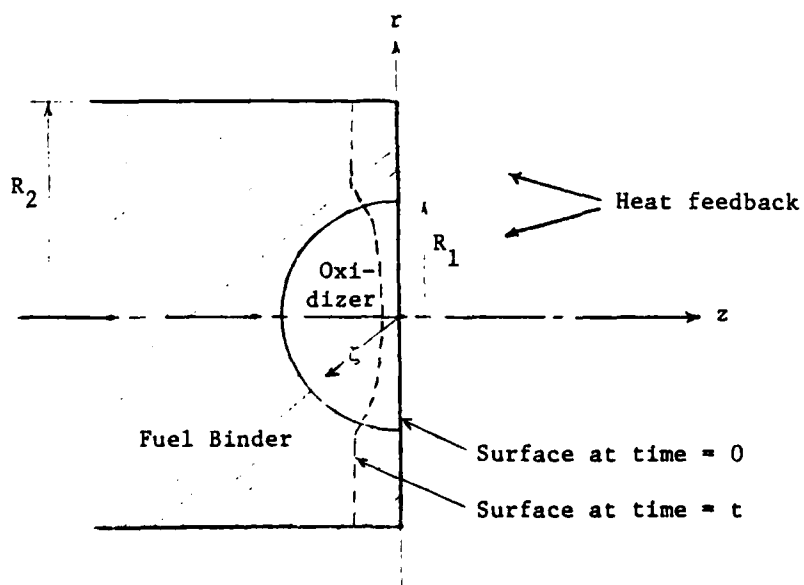


Fig. 3 Modified Cross-sectional View of a Statistically Averaged Element Considered in the Ignition Model

interface, and partly absorbed in depth in the solid phase. Some of the in-depth absorption of radiation can cause photochemical decomposition and some radiation is emitted by the surface to the surroundings. Because of external heat deposition (by radiation or by hot gases in the surroundings), the fuel and oxidizer begin to gasify when the gasification temperature of each individual component is reached. The gasified fuel and oxidizer diffuse in the surroundings; the ambient oxidizer may diffuse toward the interface and eventually, following the mixing of these gases, there is an exothermic reaction in the gas phase. Simultaneously, the sub-surface and heterogeneous reactions may continue. Heat evolved and absorbed from all of these reactions is redistributed by conduction, convection, radiation, and mass diffusion. Eventually, thermal runaway is reached at any of the solid, gas, or interface sites. The ignition criterion then determines the location and instant of ignition. The above process is described by the following mathematical formulation.

3.1.3 Governing Equations

Equations (1) through (4) represent the gas-phase continuity, energy and species equations for oxidizer and fuel gases.

Continuity equation:

$$\frac{\partial \rho_g}{\partial t} + \frac{\partial (\rho_g v_z)}{\partial z} = 0 \quad (1)$$

Energy equation:

$$c_p \rho_g \frac{\partial T}{\partial t} + \rho_g c_p v_z \frac{\partial T}{\partial z} - \frac{\partial P}{\partial t} = \frac{1}{r} \frac{\partial}{\partial r} \left(k_g r \frac{\partial T}{\partial r} \right) + \frac{\partial}{\partial z} \left(k_g \frac{\partial T}{\partial z} \right) + \dot{q}_g''' \quad (2)$$

small

Oxidizer species equation:

$$\rho_g \frac{\partial y_{O_x}}{\partial t} + \rho_g v_z \frac{\partial y_{O_x}}{\partial z} = \frac{1}{r} \frac{\partial}{\partial r} \left(r \rho_g \frac{\partial y_{O_x}}{\partial r} \right) + \dot{\omega}_{O_x}''' \quad (3)$$

Fuel species equation:

$$\rho_g \frac{\partial Y_F}{\partial t} + \rho_g v_z \frac{\partial Y_F}{\partial z} = \frac{1}{r} \frac{\partial}{\partial r} (r D \rho_g \frac{\partial Y_F}{\partial r}) + \dot{\omega}_F''' \quad (4)$$

The inhomogeneous terms \dot{q}_g''' , $\dot{\omega}_{O_x}'''$, and $\dot{\omega}_F'''$ will be discussed later.

Since the region of interest in the gas phase during the ignition process is very small (in the order of 1 mm), local pressure in this region is considered to be spatially uniform. However, the pressure is allowed to vary with respect to time. The pressure-time relationship is assumed to be known either from a measured P-t trace or a prescribed pressure-time information simulating any ignition process. Therefore, the gas-phase momentum equations are reduced to

$$P = P(t) \quad (5)$$

Because pressure is usually not extremely high during the ignition interval, the perfect gas law can be used as the equation of state,

$$\rho_g = \frac{P}{RT} \quad (6)$$

Because of the heterogeneous nature of the propellants, separate energy equations are written for oxidizer and fuel binder in the solid phase, as shown in Equations (7) and (8). The two equations govern the variation of temperature distribution in different regions with different thermal properties.

For oxidizer:

$$\rho_{O_x,s} c_{O_x,s} \frac{\partial T}{\partial t} = [k_{O_x,s} \frac{\partial^2 T}{\partial z^2} + k_{O_x,s} \frac{\partial^2 T}{\partial r^2} + \frac{k_{O_x,s}}{r} \frac{\partial T}{\partial r}] + \dot{q}_{O_x,s}''' \quad (7)$$

For fuel binder: $\rho_{F,s} c_{F,s} \frac{\partial T}{\partial t} = [k_{F,s} \frac{\partial^2 T}{\partial z^2} + k_{F,s} \frac{\partial^2 T}{\partial r^2} + \frac{k_{F,s}}{r} \frac{\partial T}{\partial r}] + \dot{q}_{F,s}''' \quad (8)$

where $\dot{q}_{O_x,s}''' = \dot{q}_{O_x,s}'''_{\text{radiation}} + \dot{q}_{O_x,s}'''_{\text{photochemical}} + \dot{q}_{O_x,s}'''_{\text{pyrolysis}} \quad (9)$

$$\dot{q}_{Ox, radiation}''' = \tau_{Ox} G \beta_{Ox} e^{-\beta_{Ox} z} = \beta_{Ox} I_z \quad (10)$$

$$\dot{q}_{Ox, photochemical}''' = \int_0^{\infty} \tau_{Ox} I_z Q_{Ox, pc, \lambda} n_{Ox, \lambda} d\lambda \quad (11)$$

(following Ohlemiller and Summerfield, 1968)

$$\dot{q}_{Ox, pyrolysis}''' = -A_{Ox, py} Q_{Ox, py} \exp(-E_{Ox, py}/R_u T) \quad (12)$$

(following Ohlemiller and Summerfield⁶, 1968)

3.1.4 Initial and Boundary Conditions

The above governing equations are subjected to a number of initial and boundary conditions. The following table summarizes the initial and boundary conditions needed for the solution of gas-phase equations.

Table 1 Initial and Boundary Conditions for Gas Phase

#	Equation	Major Dependent Variable	Independent Variables for BC and IC	Subtotal of IC and BC
1	Continuity	v_z	t, z	2
2	Energy	T	t, r, r, z, z	5
3	Species: Ox.	Y_{Ox}	t, r, r, z	4
4	Species: Fuel	Y_F	t, r, r, z	4
TOTAL (IC and BC) =				15

Initially, the ambient conditions in the gas phase and the temperature of the propellant are known, therefore, at $t = 0$ for the gas phase, we have

$$v_z(0,r,z) = 0, \quad T(0,r,z) = T_{g,i}, \quad (13)$$

$$Y_{Ox}(0,r,z) = Y_{Ox,i}, \quad Y_F(0,r,z) = Y_{F,i}$$

and for the solid phase (either for oxidizer particle or the fuel binder), we have

$$T(0,r,z) = T_i. \quad (14)$$

The boundary conditions far away from the gas-solid interface are:

$$T(t,r,\infty) = T_{g,\infty}(t) \quad (15)$$

and
$$T(t,r,-\infty) = T_i \quad (16)$$

for gas and solid phases, respectively.

The symmetry conditions along the centerline of the statistically averaged propellant element (see Figure 3) under consideration are

$$\left. \begin{aligned} \frac{\partial Y_{Ox}}{\partial r}(t,0,z) &= 0 \\ \frac{\partial Y_F}{\partial r}(t,0,z) &= 0 \\ \frac{\partial T}{\partial r}(t,0,z) &= 0 \end{aligned} \right\} \text{in gas phase} \quad (17)$$

and

$$\frac{\partial T}{\partial r}(t,0,z) = 0 \quad \text{in solid phase} \quad (18)$$

At the outer surface of the element adiabatic condition can be applied, since identical elements are assumed to be around this element. Therefore,

$$\left. \begin{aligned} \frac{\partial Y_{Ox}}{\partial r}(t, R_2, z) &= 0 \\ \frac{\partial Y_F}{\partial r}(t, R_2, z) &= 0 \\ \frac{\partial T}{\partial r}(t, R_2, z) &= 0 \end{aligned} \right\} \text{in gas phase} \quad (19)$$

and

$$\frac{\partial T}{\partial r}(t, R_2, z) = 0 \quad \text{in solid phase.} \quad (20)$$

The oxidizer mass flux balance across the interface between the oxidizer particle and gas phase, i.e. $z = z_{Ox-g}$, is given by

$$\rho_g v_z Y_{Ox} \Big|_{z_{Ox-g}^-} = \rho_g v_z Y_{Ox} \Big|_{z_{Ox-g}^+} - \rho_g D \frac{\partial Y_{Ox}}{\partial z} \Big|_{z_{Ox-g}^+} + \dot{\omega}_{Ox} \quad (21)$$

and that across the interface between the fuel and gas phase, i.e. $z = z_{F-g}$, is given by

$$0 = \rho_g v_z Y_{Ox} \Big|_{z_{F-g}^+} - \rho_g D \frac{\partial Y_{Ox}}{\partial z} \Big|_{z_{F-g}^+} + \dot{\omega}_{Ox} \quad (22)$$

The fuel mass flux balance across the interface between the oxidizer particle and gas phase, i.e. $z = z_{Ox-g}$, is given by

$$0 = \rho_g v_z Y_F \Big|_{z_{Ox-g}^+} - \rho_g D \frac{\partial Y_F}{\partial z} \Big|_{z_{Ox-g}^+} + \dot{\omega}_F \quad (23)$$

and that across the interface between the fuel and gas phase, i.e. $z = z_{F-g}$, is given by

$$\rho_g v_z Y_F \Big|_{z_{F-g}^-} = \rho_g v_z Y_F \Big|_{z_{F-g}^+} - \rho_g D \frac{\partial Y_F}{\partial z} \Big|_{z_{F-g}^+} + \dot{\omega}_F \quad (24)$$

Since the temperature must be continuous at the gas-solid interface, we have

and

$$T \Big|_{z_{F-g}^+} = T \Big|_{z_{F-g}^-} \quad (25)$$

$$T \Big|_{z_{Ox-g}^+} = T \Big|_{z_{Ox-g}^-}$$

The energy flux balance across the oxidizer-gas interface, i.e. $z = z_{Ox-g}$, is given by

$$k_{Ox,s} \frac{\partial T}{\partial z} \Big|_{z_{Ox-g}^+} = k_g \frac{\partial T}{\partial z} \Big|_{z_{Ox-g}^+} + \alpha_{Ox-g} G - \epsilon_{Ox} E_{b_{Ox}}$$

(conductive heat flux into the oxidizer) (conductive heat flux from gas phase) (radiation absorption at the surface) (radiation loss from the surface)

$$+ r_{b_{Ox}} \rho_{Ox,s} T (c_{Ox,s} - c_{p,g}) + \dot{q}''_{Ox-g} \quad (26)$$

(net convective heat flux into the interface) (net heat generation at the surface)

and that across the fuel-gas interface, i.e. $z = z_{F-g}$, is given by

$$k_{F,s} \frac{\partial T}{\partial z} \Big|_{z_{F-g}^+} = k_g \frac{\partial T}{\partial z} \Big|_{z_{F-g}^-} + \alpha_{F-g} G - \epsilon_F E_{b_F}$$

(conductive heat flux into the fuel) (conductive heat flux from the gas phase) (radiation absorption at the surface) (radiation loss from the surface)

$$+ r_{b_F} \rho_{F,s} T (c_{F,s} - c_{p,g}) + \dot{q}''_{F-g} \quad (27)$$

(net convective heat flux into the interface) (net heat generation at the surface)

At the oxidizer-fuel interface, $\zeta \equiv \sqrt{r^2 + z^2} = R_1$, the energy flux balance is

$$\begin{aligned}
 -k_{F,s} \left. \frac{\partial T}{\partial \zeta} \right|_{R_1^+} &= -k_{Ox,s} \left. \frac{\partial T}{\partial \zeta} \right|_{R_1^-} + \dot{q}_{Ox-F}'' \\
 &+ \alpha_{Ox-F} \tau_{Ox} G e^{-\beta_{Ox} z} \\
 &\text{(radiation absorption at the interface)}
 \end{aligned} \tag{28}$$

(conductive heat flux into the fuel) (conductive heat flux from the oxidizer) (net heat generation at the surface)

At the $\zeta \equiv \sqrt{r^2 + z^2} = R_1$ interface, the temperature continuity is

$$T \Big|_{R_1^+} = T \Big|_{R_1^-} \tag{29}$$

The mass continuity across the oxidizer-gas interface relates the local gas velocity to the regression rate of the oxidizer by the following relationship.

$$\rho_g v_z \Big|_{z_{Ox-g}^+} = \rho_{Ox} r_{b_{Ox}} \tag{30}$$

similarly for fuel we have

$$\rho_g v_z \Big|_{z_{F-g}^+} = \rho_F r_{b_F} \tag{31}$$

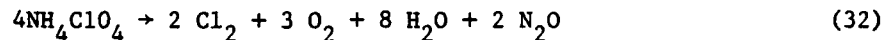
3.1.5 Chemical Kinetics Information

In order to close the model proposed above, the following terms must be expressed in terms of the dependent and independent variables $r_{b_{Ox}}$, r_{b_F} , \dot{q}_g'' , $\dot{\omega}_{Ox}''$, $\dot{\omega}_F''$, \dot{q}_{Ox-F}'' , \dot{q}_{F-g}'' , $\dot{\omega}_{Ox}''$, and $\dot{\omega}_F''$. For this purpose, knowledge of detailed chemical reactions and kinetic data is necessary. A survey of kinetic information was therefore conducted to obtain thermal decomposition data (rate

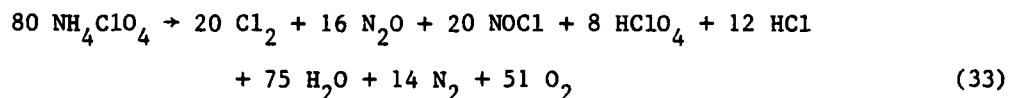
constants, physical constants for melting and ablation, etc.), and to determine the key steps in a chemical reaction mechanism, a process which is usually extremely complicated. In particular, kinetic information was sought for AP, PBAA, HMX, RDX, and NC/NG; a summary of the information obtained for each of the ingredients follows.

(a) AP (Ammonium Perchlorate)

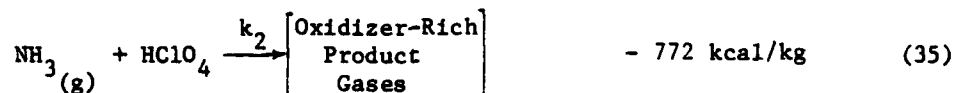
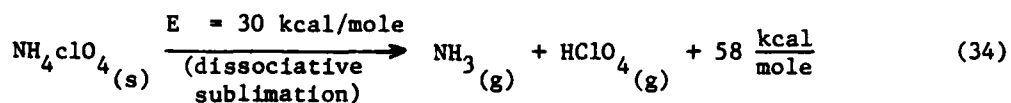
AP is the most widely used oxidizer in composite solid propellants. Most of the following information was obtained from Guirao and Williams;⁷ however, many of the values were collected from and confirmed by other sources.⁸⁻¹¹ Briefly, the overall burning of AP involves first the dissociative sublimation into ammonia and perchloric acid, which begins around 473K and is an endothermic process. The perchloric acid then decomposes in the gas phase at higher temperatures (above 523K), and reacts with ammonia exothermically. The products of this reaction are oxidizer-rich gases which react with fuel gases vaporized from fuel binders of a composite propellant. For temperatures between 473 and 573K, the thermal decomposition of AP can be represented by⁸



The reaction for decomposition above 623K is



These reactions are exothermic, and are believed to be preceded by dissociative sublimation^{7,9} of AP as shown below.



where

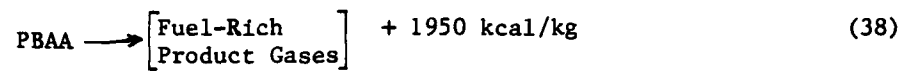
$$\frac{d[\text{HClO}_4]}{dt} = -k_2 [\text{HClO}_4][\text{NH}_3] \quad (36)$$

$$k_2 = A_{g_2} T \exp\left(-\frac{E_{g_2}}{R_u T}\right) \quad (37)$$

$$E_{g_2} = 15.47 \text{ kcal/mole}, A_{g_2} = 2.03 \times 10^{11} \text{ cm}^3/\text{mole-s-k}$$

(b) PBAA (Polybutadiene Acrylic Acid)

PBAA is a fuel binder used with AP in many composite propellants. PBAA is usually cured with EPON. The fuel binder made with 86.6% PBAA and 14.4% EPON828 is represented⁹ by the formula $\text{CH}_{1.535}\text{O}_{0.03873}$. The thermal decomposition of PBAA begins around 610K and continues until 770K.¹² According to Varney and Strahle,¹² the decomposition can be written as



$$\frac{d \ln M_{\text{PBAA}}}{dt} = - A \exp \left[- \frac{E}{R_u T} \right] \quad (39)$$

where

$$E = 34 \text{ kcal/mole}$$

$$A = 2 \times 10^7 \text{ s}^{-1}$$

(c) HMX (Cyclotetramethylenetetranitramine)

The principal products of HMX decomposition are formaldehyde (HCHO), nitrogen oxide (N_2O), hydrogen cyanide (HCN), and nitrogen dioxide (NO_2).¹³ The currently understood chemical kinetic processes between these principal products are given below.



Corresponding rates of depletion of NO_2 and N_2O of the above from reactions are given below.

$$-\frac{d(NO_2)}{dt} = 1.26 \times 10^{13} \exp(26700/R_u T) (Ar)^{.40} (HCHO)^{.56} (NO_2)^{.90} \text{ mole/cm}^3 \text{ sec}$$

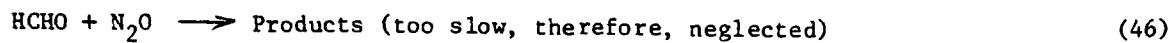
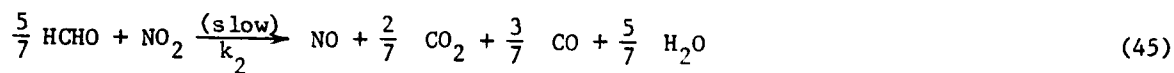
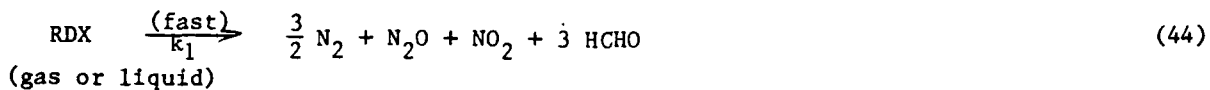
$$-\frac{d(N_2O)}{dt} = 8.41 \times 10^{11} \exp(-27400/R_u T) (Ar)^{-.14} (HCHO)^{.64} (N_2O)^{1.17} \text{ mole/cm}^3 \text{ sec}$$

$$-\frac{d(NO_2)}{dt} = 4.9 \times 10^{11} \exp(-43300/R_u T) (Ar)^{1.03} (HCN)^{-.03} (NO_2)^{.65} \text{ mole/cm}^3 \text{ sec}$$

$$-\frac{d(N_2O)}{dt} = \text{not known}$$

(d) RDX (Cyclotrimethylenetrinitramine)

According to Ben Reuven et al.,¹⁴ the decomposition of RDX can be represented by the following reactions.



$$k_1(\text{liquid}) = 3 \times 10^{18} \exp(-47500/R_u T), \text{ sec}^{-1} \quad (47)$$

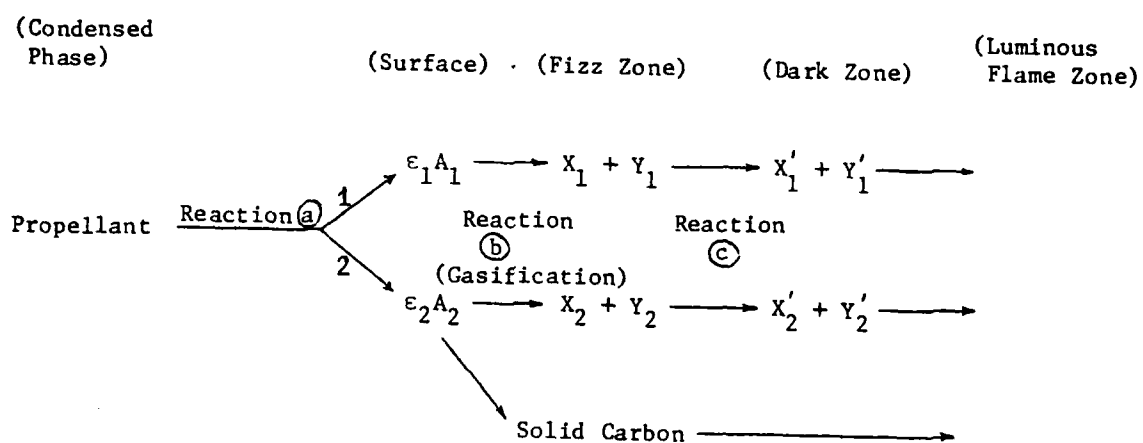
$$k_1(\text{gas}) = 10^{15.5} \exp(-41500/R_u T), \text{ sec}^{-1}$$

$$k_2 = 10^{12} \exp(-19000/R_u T), \text{ cm}^3/\text{gmol-sec}, T > 430 \text{ K} \quad (48)$$

$$k_2 = 10^{13.1} \exp(-26700/R_u T), \text{ cm}^3/\text{gmol-sec}, 970\text{K} < T < 1470\text{K}$$

(e) Double-Base Propellants

According to Kubota et al.,¹⁵ the chemical kinetic processes in decomposition and the reaction of double-base propellants can be represented by the following mechanism.



Path 1 only : Noncatalyzed reaction scheme

Paths 1 and 2 : Catalyzed reaction scheme

ϵ_1, ϵ_2 : Mass fractions of the propellant, $\epsilon_1 + \epsilon_2 = 1$

A : Products after decomposition

X, Y : Chemical species in gas phase

Z : Pre-exponential factor

$$E_a = 5 \times 10^3 \text{ cal/mole}$$

$$Z_a = 5 \times 10^6 \text{ cm}^3/\text{g-sec}$$

$$E_{b_1} = 17 \times 10^3 \text{ cal/mole}$$

$$Z_{b_1} = 5 \times 10^5 \text{ cm/sec (?)}$$

$$E_{b_2} = 17 \times 10^3 \text{ cal/mole}$$

$$Z_{b_2} = 5 \times 10^5 \text{ cm/sec}$$

$$E_{c_1} = 17 \times 10^3 \text{ cal/mole}$$

$$Z_{c_1} = 1 \times 10^9 \text{ cm}^3/\text{g-sec}$$

$$E_{c_2} = 7.7 \times 10^3 \text{ cal/mole}$$

$$Z_{c_2} = 1 \times 10^9 \text{ cm}^3/\text{g-sec}$$

In the above summary of kinetic information, some of the detailed intermediate and chain reactions are not given. One reason for omitting them is that these detailed chain reactions are usually proposed reaction mechanisms which have not been verified and therefore may be unreliable. It was apparent from this survey that kinetic information in general is incomplete and scattered. Because of the inadequacy of relevant kinetic data and the mathematical intricacy involved in consideration of detailed kinetics, it is prudent at this time to consider a single-step, global reaction between the oxidizer-rich and fuel-rich gases for determining gas-phase heat release. However, realistic rate equations for the decomposition of oxidizer particle and fuel binder are taken into consideration in the model.

AP/PBAA composite propellant is considered, in the solution of the proposed ignition model for the following reasons: 1) a number of experiments have been performed and are in progress on this propellant; and 2) reliable kinetic information is available for this propellant. Numerical solution which uses AP/PBAA propellant data is in progress.

3.2 Investigation of Combustion/Solid Mechanics Interaction in Narrow Cracks

Of the several interdependent gas dynamic and solid mechanics processes that may influence combustion behavior in a propellant crack, the coupling between the pressure along the crack and the deformation was considered to be the most important. The analysis considers deformations caused by both pressure loading and burning. Other coupled processes such as thermal stresses due to the temperature gradient in the solid, variation in burning rate due to compression of the propellant, etc., were considered to be of secondary importance and were ignored in the present analysis.

The general layout of the computer program is shown in Figure 4. The theoretical coupling considered between the convective burning and structural analysis is simplified, as discussed previously, to the transfer of pressure loading and crack deformation. Pressure is calculated by the gas dynamic portion of the computer program at each nodal point location on a one-dimensional grid along the length of the crack. The convective burning analysis of the crack combustion incorporates the crack geometry variation caused by both mechanical deformation and mass loss through gasification of the propellant at the surface. Once the gas-phase equations are solved, and pressures and burning rate along the crack are calculated for a particular time t , program control is transferred to the nonlinear finite-element analysis program (NFAP) portion of the combined code. NFAP reformulates the geometry because of the material loss, and updates the stiffness matrix for the new time step. Surface elements of the finite-element mesh are loaded with the pressure obtained through the gas-phase equations. The propellant deformation is calculated in NFAP, using a static analysis at time t . A plane-strain analysis is used to solve general stress-strain equations; this is congruous to the experimental test configuration. The transient nature of the pressure loading is considered by using a static analysis at incremental time steps.

Figure 5 is a diagram of the finite-element grids used for structure analysis and the finite-difference nodes used for gas-phase solutions. The configuration is compatible with the geometry considered in the theoretical model, as well as with that used in the experiments. Two-dimensional, eight-node, isoparametric, quadrilateral elements were used to model a sample crack. Because of symmetry, only half of the crack needs to be considered. Of the eight nodes in an element, four are located at the corners, and one at the midpoint of each side. Except near the tip region, the finite-difference nodes used for the gas-phase solution

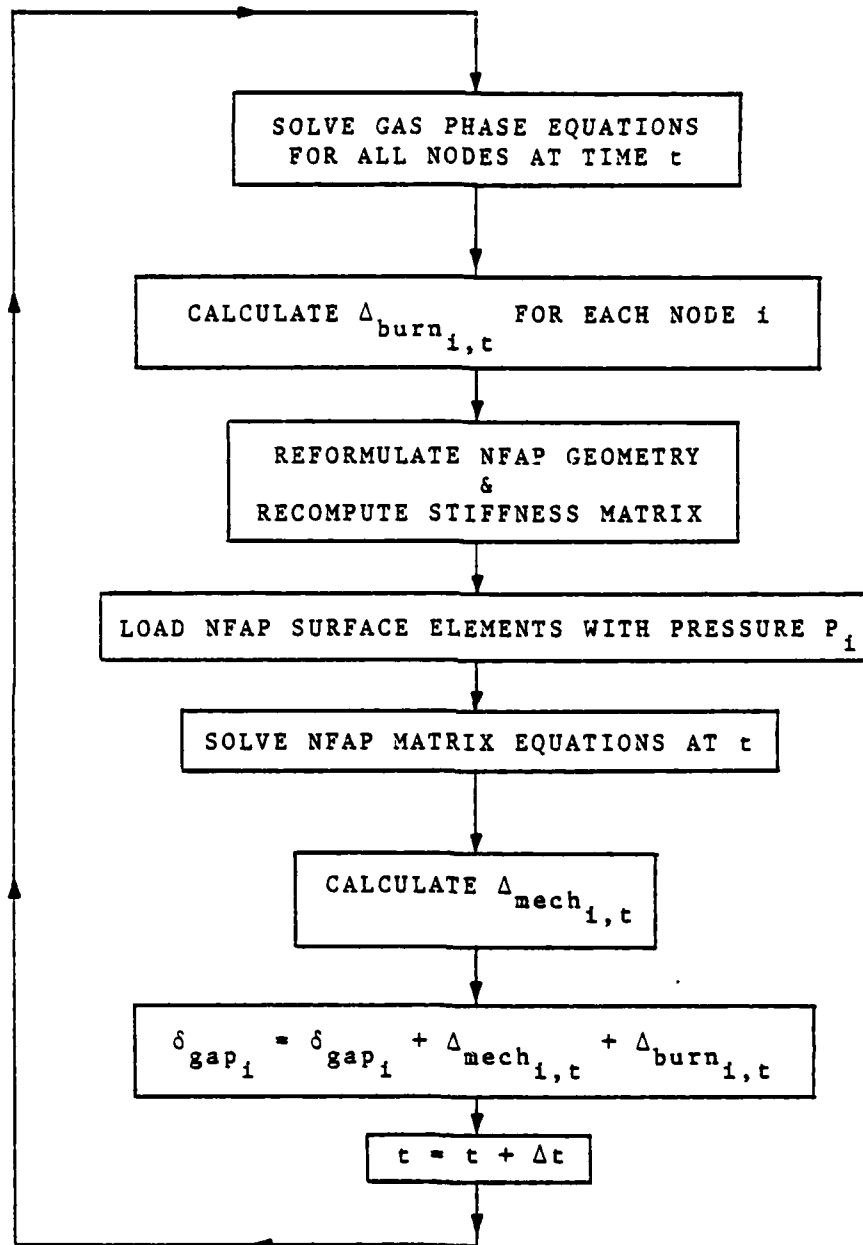


Fig. 4 General Layout of Coupled Combustion/Solid Mechanics Computer Program

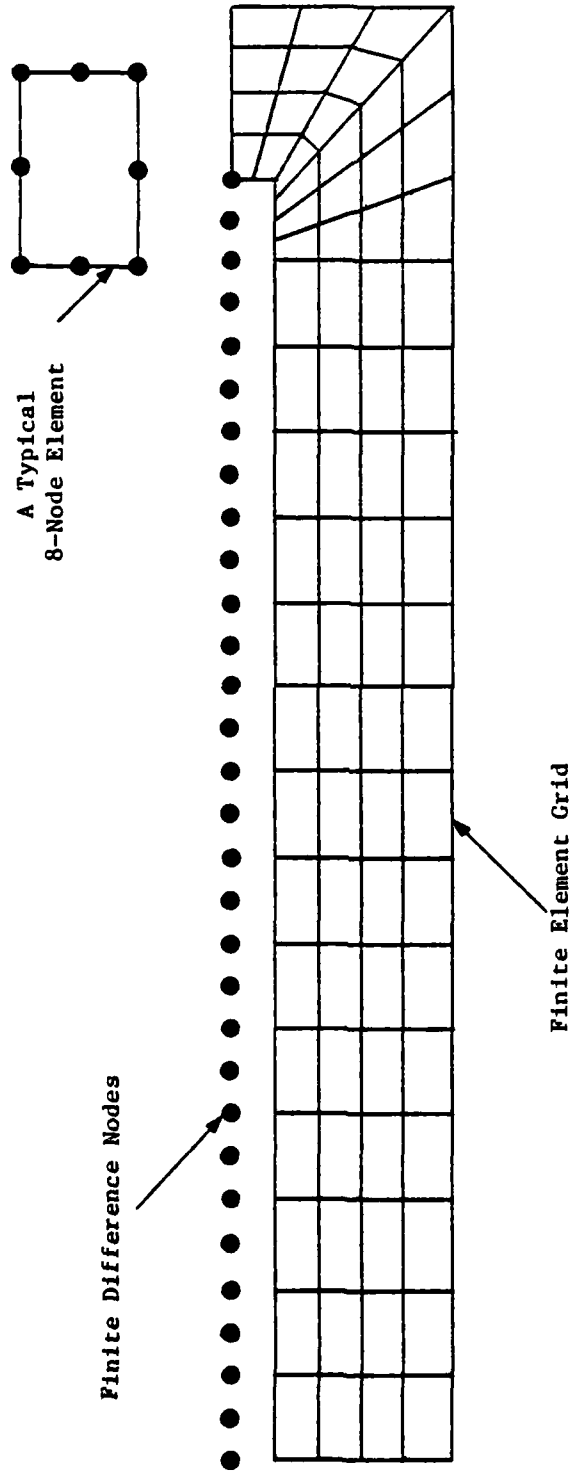


Fig. 5 Finite Element Grid and Finite Difference Nodes

are in a one-to-one correspondence with the finite-element nodes which form the propellant surface in the two-dimensional structural analysis mesh. This is helpful in reducing the computational effort in transferring the values from finite-difference nodes to finite-element grids, and vice versa.

Figures 6 and 7 show calculated pressure distributions at various times for cases in which propellant deformation becomes very important. For results shown in Figure 6 (Case 1), the chamber pressurization rate was 3.8×10^5 atm/s and the gap width was 0.51 mm. Only those curves of interest are shown, and for ease of explanation, they are not super-imposed. Between $t = 0.25$ and $.275$ ms, the crack gap near the entrance is partially closed, causing a local peak near the entrance; however, pressure at the crack entrance is identical to that in the chamber. At $t = 0.3$ ms, high pressure in the chamber and at the crack entrance cause the closure to move to $x/L = 0.1$, resulting in a local pressure peak. The localized high pressure at $x/L = 0.1$ causes the propellant to deform; the region of gap closure moves to $x/L = 0.2$, resulting in a substantial increase of local pressure. The subsequent closure results in a zero gap width and causes the gas-dynamic solution to explode. This predicted movement of the partial gap closure is very similar to that observed experimentally (see Figure 11).

Case 2, shown in Figure 7, was computed for a higher pressurization rate of 5×10^5 atm/s and a wider initial gap width of .89 mm. At 0.45 ms (not shown in the Figure), gap closure occurs near the crack entrance, resulting in localized high pressure near the entrance. Again, both the high pressure near the entrance in the cavity and that acting on the side walls exposed to the chamber cause the gap closure to move downstream, resulting in a pressure peak near $x/L = 0.17$ (at .475 ms). At 0.5 ms, two regions of gap closures are obtained, resulting in pressure peaks at $x/L = 0.1$ and 0.27 , respectively. As time passes, the

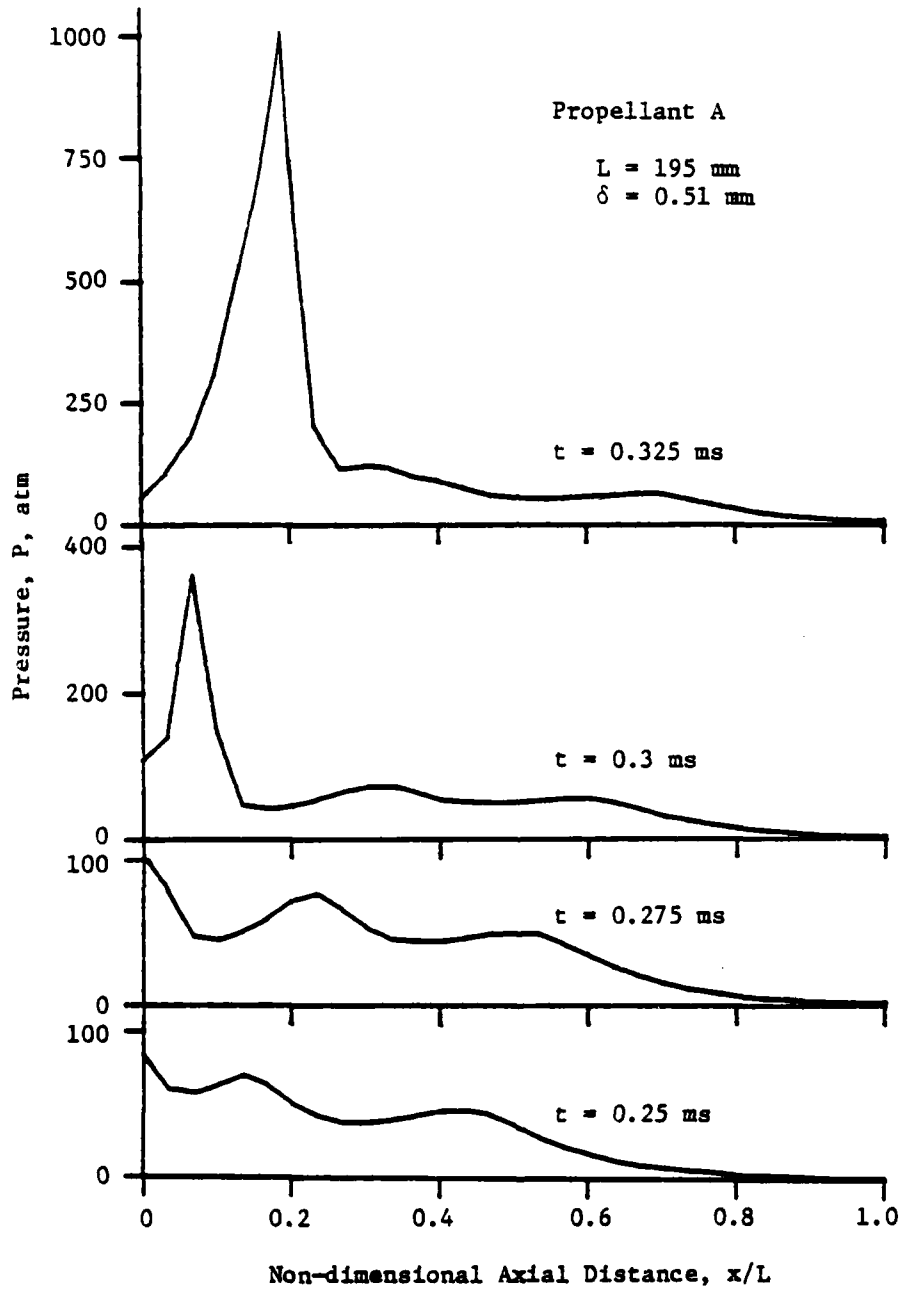


Fig. 6 Calculated Pressure Distribution at Various Times during Crack-Gap Closure (Case 1)

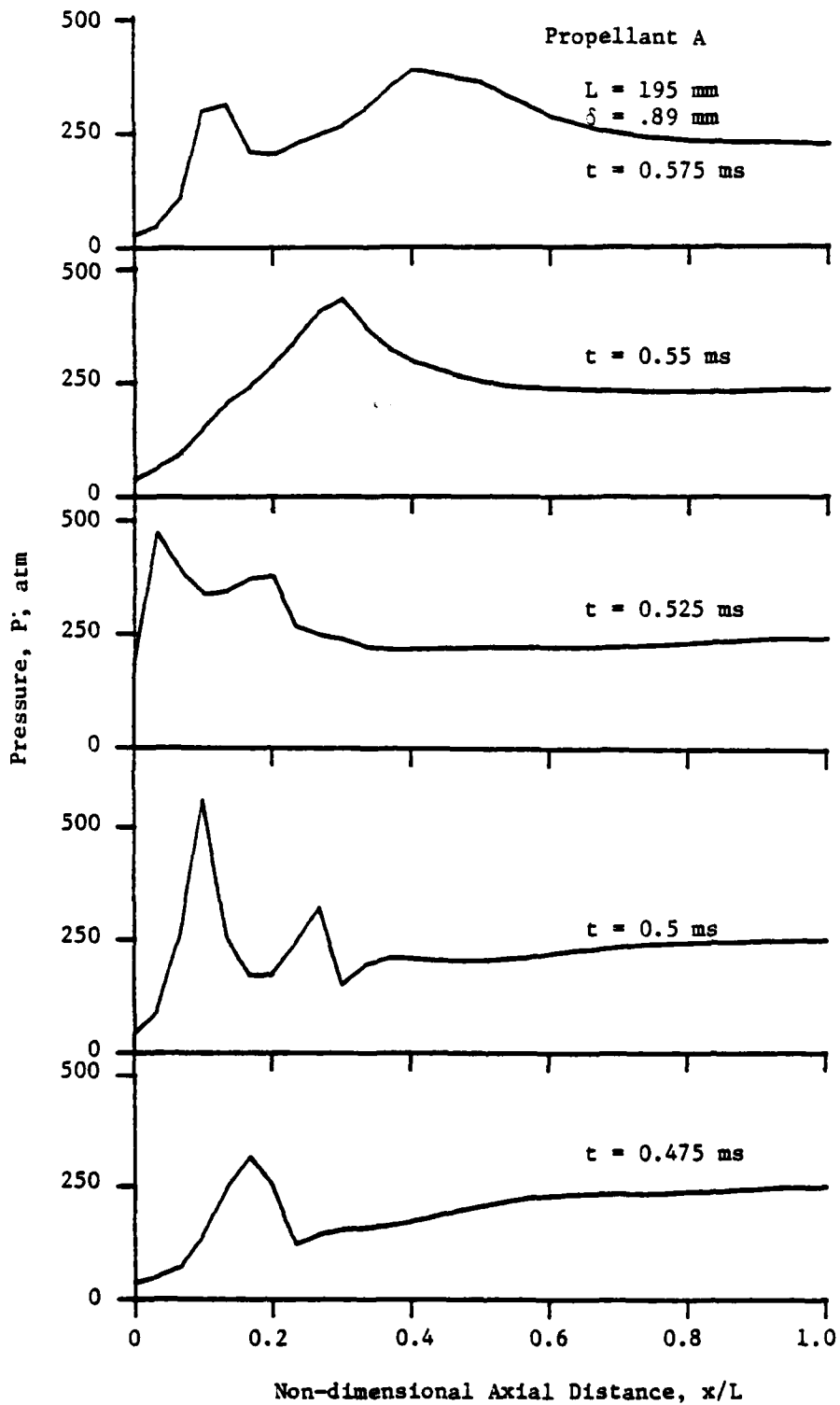


Fig. 7 Calculated Pressure Distribution at Various Times during Crack-Gap Closure (Case 2)

pressure peaks move downstream; some disappear as a result of propellant deformation. At 0.525 ms, another gap closure develops near the entrance. This process continues as time progresses. Once again, these results explain the behavior of the gap closures observed experimentally.

Results obtained here indicate that closure of the crack gap, which may initially occur at the crack entrance because of small gap widths and high chamber pressures, may propagate along the crack and result in local pressure peaks. The gap closure is not observed for cracks with large gap widths or at low chamber pressures because propellant deformation under these conditions is small and does not affect the ignition process substantially. Detailed governing equations and verification for the structure mechanics part is given in Ref. 16. A paper, which includes a more detailed analysis of the combined program, has been accepted for the JANNAF Propulsion Systems Hazards Subcommittee Meeting (Ref. 17). Abstracts of these papers are given in Appendices II and III, respectively.

IV. EXPERIMENTAL WORK

4.1 Development of a New Igniter System

A new igniter system has been designed and fabricated to obtain higher pressurization rates ($>10^5$ atm/s) in the test chamber. The system employs an electric primer (FA 874) as the initiator for ignition of a propellant charge which is used as a source for hot gas generation. Using electric primers instead of percussion primers ensures higher reliability and greater reproducibility. Numerous test firings have been conducted to evaluate the effect of different types of igniter-propellant charges on the rate of pressurization. An ignition circuit has also been designed and successfully used for activating electric primers.

4.2 Improvements in Data Acquisition System

The ignition process of solid propellants under highly transient pressure excursion is usually of short duration (in the order of a few hundred microseconds). To achieve better time resolution, a multichannel transient waveform recorder (Physical Data Model #515.234) was ordered in the beginning of the contract. This device, received in January 1980, is being used, together with a magnetic tape recorder (Hewlett Packard Model 3955 B), to record transient signals. The maximum sampling rate of the Physical Data System is 2×10^6 samples/sec, and the maximum amplitude resolution is 0.1%. To obtain more detailed information of the ignition event, the $\frac{1}{2}$ -frame optical head was replaced by a $\frac{1}{4}$ -frame optical head. Currently, the highest framing rate is about 40,000 pictures per second. For extremely rapid ignition events, streak photography was used. To measure the instantaneous heat flux at the simulated propellant surface, a set of thin film (0.5 to 1 μm) Rhodium-Platinum heat-flux gages (Medtherm 302) was ordered and received only recently. These gages have microsecond response time for

temperature measurements. Due to the delay in receiving the heat-flux gages, measurements have not yet been carried out. Modifications are being made in the chamber in order to install the flux gage.

4.3 Experimental Observations of Flame Spreading and Combustion in Narrow Cracks

An improved procedure for sample preparations has been developed to observe and record flame-spreading and ignition processes in narrow propellant cracks. A schematic diagram of the test chamber and igniter system for this study is given in Figure 8. A crack was formed between a propellant slab and the sacrificial plexiglass window, i.e., one side of the crack was an inert, transparent, plexiglass window, and the other was a propellant slab glued to a stainless steel base plate. This type of configuration provided direct (front view) observation of the flame-front propagation process. Figure 9 shows a typical propellant sample used for detailed observation of the flame front. The gap width of such a crack configuration is varied by the amount by which the propellant surface is recessed below the side-leg assembly (see Figure 9). The propellant slabs used in these tests were 183 mm long and 17.7 mm wide. Figure 10 gives a block diagram of the data acquisition system.

Figure 11 presents a sequence of pictures of a test performed on a narrow crack (gap width = 455 μm) in which the crack was formed between the propellant surface and the plexiglass window. It is interesting to note that when the width of the crack gap is very small (500 μm or smaller), partial closure of the crack occurs because of propellant deformation. Partial closure first appears near the entrance. As time progresses, the closure region moves downstream and a second partial closure region develops near the entrance. At times, as the process continues three or four such partial closures are observed simultaneously (for initial gap widths of the order of 450 μm). Usually, at the moment at which

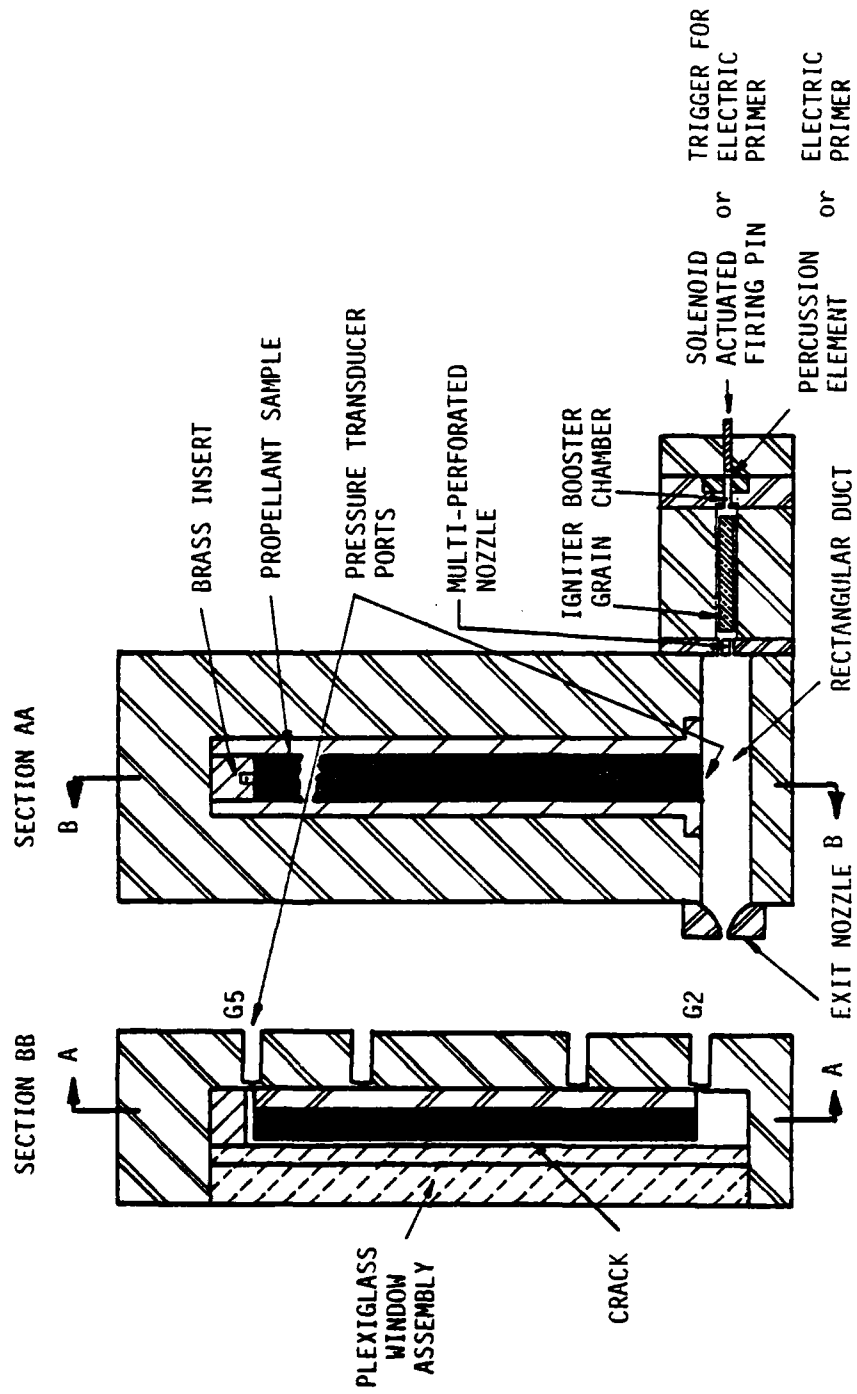


Fig. 8 Schematic Diagram of Crack Combustion and Igniter System

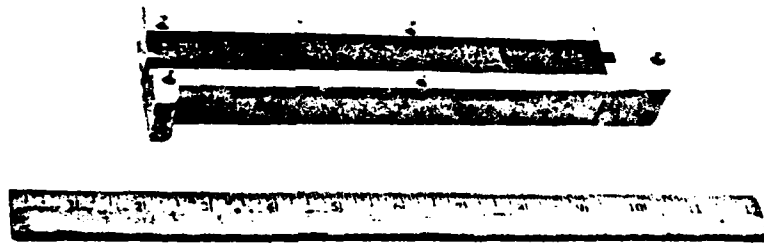


Fig. 9 Propellant Sample Used for Detailed Observation of
Flame Front

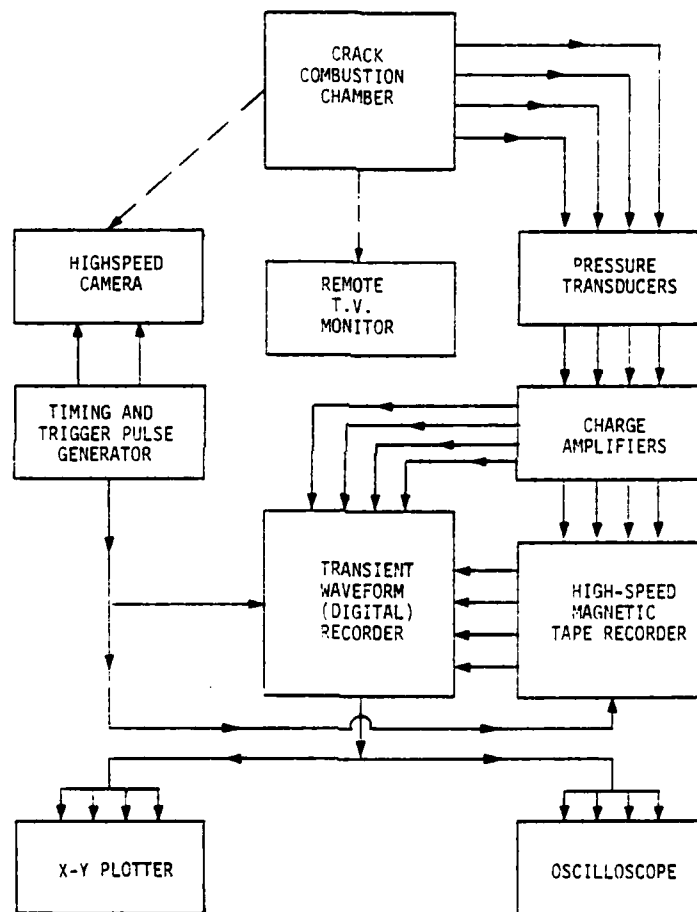
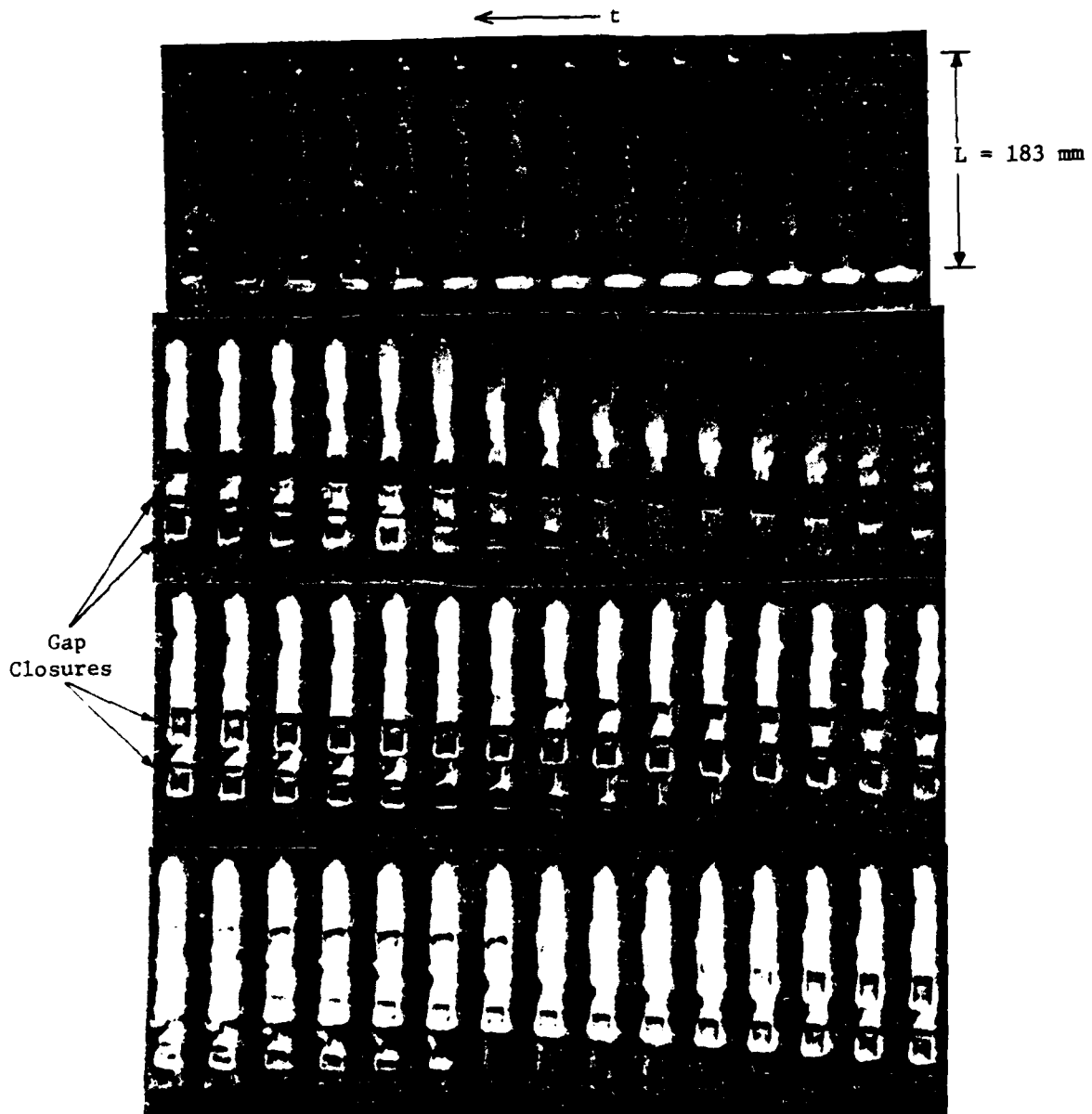


Fig. 10 Block Diagram of Data Acquisition System



Framing Rate = 36,700 Pictures Per Second

Fig. 11 A Sequence of Photographs Showing Crack-Gap Closures

the third closure develops at the entrance, the second and first regions are located, respectively, at approximately 20% and 50% of the crack length from the entrance. Later, as the combustion process becomes more pronounced, the partial closure regions disappear as a result of both propellant regression and higher pressure in the crack cavity. The entire process is believed to be the result of deformations caused by high pressure acting on the propellant surface exposed to the chamber, and by complex interaction between propellant deformation and pressure distribution in the crack cavity. This implies that the coupling between chamber pressurization, crack combustion, and propellant deformation is quite important, especially in the case of very narrow cracks.

Tests were continued to study the effect of pressurization rate, propellant type, crack-gap width, and crack length on flame-spreading and combustion processes in solid propellant cracks. Details of the procedure and the results are given in Ref. 18. The abstract for the paper is given in Appendix IV.

V. NOMENCLATURE

A	frequency factor
c, c_p	specific heat
D	binary mass diffusion coefficient
E	activation energy
E_b	black body radiation intensity
G	external radiation heat flux
I_z	local radiation flux at z
k	thermal conductivity
k_1, k_2	rate constants for reactions 1 and 2
P	pressure
\dot{q}''	heat flux (energy per unit time per unit area)
\dot{q}'''	heat generation rate (energy per unit time per unit volume)
$Q_{pc\lambda}$	rate of heat generation due to photochemical process per unit wavelength/local radiation flux at z
Q_{py}	heat of pyrolysis per unit mass
r	radial distance from the center of the statistically averaged element
r_b	burning rate
R	gas constant
R_u	universal gas constant
R_1, R_2	radii of outer surfaces of oxidizer particle and fuel binder, respectively
t	time
v_z	gas phase velocity in z direction
Y_i	mass fraction of species i in the gas phase
z	distance from the initial (t=0) position of the interface; positive in the gas phase

α	radiation absorptivity of the interface
β	in-depth radiation absorption coefficient
ϵ	emissivity of the interface
ζ	radial distance of the spherical coordinate, $\sqrt{r^2 + z^2}$
η_λ	efficiency for photochemical process at wavelength λ
λ	wavelength of external radiation
ρ	density
τ	transmissivity of the solid phase
$\dot{\omega}''$	mass production rate per unit area
$\dot{\omega}_i'''$	mass production rate per unit volume

Subscripts

1,2,a,b,c	various reactions
F	fuel
F-g	fuel-gas interface
g	gas phase
i	initial value or species i
Ox	oxidizer
Ox-F	oxidizer-fuel interface
Ox-g	oxidizer-gas interface
pc	photochemical
py	pyrolysis
s	solid phase
z	in z direction (perpendicular to the initial position of the interface)
∞	far away from the interface in z direction
λ	wavelength

VI. REFERENCES

1. Price, E. W., Bradley, H. H., Jr., Dehority, G., L., and Ibiricu, M. M., "Theory of Ignition of Solid Propellants," AIAA Journal, Vol. 4, Sept. 1966, pp. 1153-1181.
2. Kulkarni, A. K., Kumar, M., and Kuo, K. K., "Review of Solid Propellant Ignition Studies", AIAA Paper No. 80-1210, AIAA/SAE/ASME 16th Joint Propulsion Conference, Hartford, Conn., July 1980.
3. Kumar, R. K., and Hermance, C. E., "Gas Phase Ignition Theory of a Heterogeneous Solid Propellant," Combustion Science and Technology, Vol. 4, 1972, pp. 191-196.
4. Kumar, M., and Kuo, K., "Ignition of Solid Propellant Crack Tip under Rapid Pressurizations," AIAA Journal, Vol. 18, July 1980, pp. 825-833.
5. Bradley, H. H., Jr., "A Unified Theory of Solid Propellant Ignition," NWC TP 5618, Parts 1-3, Naval Weapons Center, China Lake, Calif., Dec. 1975.
6. Ohlemiller, T. J., and Summerfield, M., "A Critical Analysis of Arc Image Ignition of Solid Propellants," AIAA Journal, Vol. 6, May 1968, pp. 878-886.
7. Guirao, C., and Williams, F. A., "A Model for Ammonium Perchlorate Deflagration between 20 and 100 atm.," AIAA Journal, Vol. 9, July 1971, pp. 1345-1356.
8. Sarner, S. F., Propellant Chemistry, Reinhold Publishing Corporation, New York, 1966.
9. Steinz, J. A., Stang, P. L., and Summerfield, M., "The Burning Mechanism of Ammonium Perchlorate-Based Composite Solid Propellants," AMS Report No. 830, Princeton University, 1969.
10. Boldyrev, V. V., Alexandrov, V. V., Boldyreva, A. V., Gritsan, V. I., Karpenko, Yu. Ya., Korobeinitchev, O. P., Panfilov, V. N., and Khaivetdinov, E. F., "On the Mechanism of the Thermal Decomposition of Ammonium Perchlorate," Combustion and Flame, Vol. 15, 1970, pp. 71-78.
11. Beckstead, M. W., Derr, R. L., and Price, C.F., "The Combustion of Solid Monopropellants and Composite Propellants," Thirteenth Symposium (International) on Combustion, The Combustion Institute, Pittsburgh, Pa., 1971, pp. 1047-1056.
12. Varney, A. M., and Strahle, W. C., "Thermal Decomposition Studies of Some Solid Propellant Binders," Combustion and Flame, Vol. 16, 1971, pp. 1-8.
13. Fifer, R. A., and Holmes, H. E., "Kinetics of Nitramine Flame Reactions," 11th JANNAF Combustion Meeting, CPIA, Sept. 1979.
14. Ben Reuven, M., Caveny, L. H., Vichnevetsky, R. J., and Summerfield, M., "Flame Zone and Sub-Surface Reaction Model for Deflagrating RDX," Sixteenth Symposium (International) on Combustion, The Combustion Institute, Pittsburgh, Pa., 1977, pp. 1223-1233.

15. Kubota, N., Ohlemiller, T. J., Caveny, L. H., and Summerfield, M., "The Mechanism of Super-Rate Burning of Catalyzed Double Base Propellants," Fifteenth Symposium (International) on Combustion, The Combustion Institute Pittsburgh, Pa., 1975, pp. 529-537.
16. Chang, T. Y., Chang, J. P., Kumar, M., and Kuo, K. K., "Combustion-Structural Interaction in a Viscoelastic Material," to be presented at Symposium on Computational Methods in Nonlinear Structural and Solid Mechanics, Washington, D.C., Oct. 6-8, 1980.
17. Kumar, M., and Kuo, K. K., "Effect of Propellant Deformation on Ignition and Combustion Processes in Solid Propellant Cracks," to be presented at the 1980 JANNAF Propulsion Systems Hazards Meeting, Monterey, Calif., Oct. 27-28, 1980.
18. Kumar, M., Kovacic, S. M., Kuo, K. K., "Gas Penetration, Flame Propagation, and Combustion Processes in Solid Propellant Cracks," AIAA Paper No. 80-1206, AIAA/SAE/ASME 16th Joint Propulsion Conference, Hartford, Conn., July 1980.

APPENDIX I

REVIEW OF SOLID-PROPELLANT IGNITION STUDIES

A. K. Kulkarni, M. Kumar, and K. K. Kuo
Department of Mechanical Engineering
The Pennsylvania State University
University Park, PA 16802

ABSTRACT (Ref. 2)

An extensive review of the literature on solid-propellant ignition has been made to establish the state of the art. Various ignition theories, experimental measurements, and ignition criteria are critically examined. The review is summarized in an easy-to-read tabular form to facilitate comparison between various studies. The effects of important parameters on ignition processes are also discussed. Major technological gaps are identified, and areas for future studies are recommended.

APPENDIX II

COMBUSTION - STRUCTURAL INTERACTION IN A VISCOELASTIC MATERIAL

T. Y. Chang and J. P. Chang
Department of Civil Engineering
The University of Akron, Akron, Ohio

M. Kumar and K. K. Kuo
Department of Mechanical Engineering
The Pennsylvania State University
University Park, Pennsylvania

ABSTRACT (Ref. 16)

The effect of interaction between combustion processes and structural deformation of solid propellant was considered. The combustion analysis was performed on the basis of deformed crack geometry, which was determined from the structural analysis. On the other hand, input data for the structural analysis, such as pressure distribution along the crack boundary and ablation velocity of the crack, were determined from the combustion analysis. The interaction analysis was conducted by combining two computer codes, a combustion analysis code and a general purpose finite element structural analysis code.

APPENDIX III

EFFECT OF PROPELLANT DEFORMATION ON IGNITION
AND COMBUSTION PROCESSES IN SOLID PROPELLANT CRACKS

M. Kumar and K. K. Kuo
Dept. of Mechanical Engineering
The Pennsylvania State University
University Park, PA 16802

To be Presented at The 1980 JANNAF
Propulsion Systems Hazards Meeting
to be held at the Naval Postgraduate
School, Monterey, California, October
27-28, 1980

ABSTRACT (Ref. 17)

In order to obtain a detailed observation of the ignition-front propagation in narrow solid propellant cracks, tests were performed on cracks formed between a propellant slab and an inert, transparent plexiglass window. Tests were conducted under rapidly increasing chamber pressure. Ignition-front propagation rates were measured using high-speed (up to 44,000 pictures per second) camera. It was observed that when the width of the crack gap is very small ($<500 \mu\text{m}$), partial closure of the crack occurs due to propellant deformation. This partial closure first appears near the entrance. As time progresses, the closure region moves downstream and a second partial closure region develops near the entrance. This process continues; at times, three or four such partial closures are observed simultaneously (for initial gap widths of the order of $450 \mu\text{m}$). Usually, at the moment when the third closure develops at the entrance, the second and first are located, respectively, at approximately 20% and 50% of the crack length from the entrance. Later as the combustion process becomes more pronounced, the partial closure regions disappear as a result of both propellant regression and higher pressure in the cavity.

The entire process is believed to be the result of deformation caused by high pressure acting on the propellant surface exposed to the chamber, and by the complex interaction between propellant deformation and pressure distribution in the crack cavity. Propellant surface exposed to the chamber are compressed by the high chamber pressure, which results in the propellant being pushed into the crack. Since during the initial pressure transient, the chamber pressure increases faster than the pressure in the crack, the propellant is pushed toward the lower pressure region inside the crack. The mechanical deformation of the propellant causes narrowing of the crack gap and consequently results in local crack closure.

The interaction between structural deformation and combustion processes was also investigated theoretically. In the theoretical model, the effect of inter-related structural deformation and combustion phenomena was taken into account by considering: a) transient one-dimensional mass, momentum and energy conservation equations in the gas phase, b) a transient one-dimensional heat conduction equation in the solid phase, and c) quasi-static deformation of the two-dimensional, linear-viscoelastic propellant crack due to pressure loading. This set of coupled, nonlinear, partial differential equations was solved numerically. The gas-dynamic equations were solved using a finite difference analysis and the structure mechanics equation was solved using a finite element analysis. Calculated results of pressure distributions at various times indicate that the effect of propellant deformation is quite important. The gap closure results in substantial local pressure peaks.

Results obtained indicate that closure of the crack gap initially occurs at the crack entrance because of small gap widths and high chamber pressures. The gap closure is not observed for cracks with large gap widths or at low chamber pressure, because propellant deformation under these conditions is small and does not affect the ignition process substantially. Gap closures and resulting pressure peaks can strongly influence the convective burning process in the crack and may contribute to the deflagration-to-detonation transition process.

APPENDIX IV

GAS PENETRATION, FLAME PROPAGATION, AND COMBUSTION PROCESSES
IN SOLID PROPELLANT CRACKS

Mridul Kumar, Stephen M. Kovacic, and Kenneth K. Kuo
The Pennsylvania State University
University Park, Pennsylvania

ABSTRACT (Ref. 18)

The effects of pressurization rate, crack-gap width, crack length, and propellant type on the ignition and flame-spreading processes in isolated AP-based solid propellant cracks have been studied experimentally. Ignition front propagation rates were measured using a high-speed (up to 44,000 pictures/second) camera. Cracks up to 200 mm in length with gap widths as low as 450 μm were studied. It was observed that the hot gases precede the ignition front. The ignition-front propagation speed increases near the crack entrance, reaches a maximum, and then decreases near the crack tip. The results of parametric study indicate that the time required for the ignition front to reach the crack tip decreases, and that the maximum velocity of the ignition front increases as the pressurization rate or burning rate of the propellant is increased. The maximum pressure in the crack increases with an increase in burning rate or crack length, but decreases with an increase in gap width. It was observed that when the crack gap width is very small ($\sim 450\mu\text{m}$), several partial closures of the crack occur due to propellant deformation caused by the strong interaction between combustion and structure mechanics.

ENERGETIC MATERIALS RESEARCHDISTRIBUTION LIST

	<u>No. Copies</u>		<u>No. Copies</u>
Assistant Secretary of the Navy (R, E, and S) Attn: Dr. R.E. Reichenbach Room 5E787 Pentagon Washington, DC 20350	1	AFATL Eglin AFB, FL 32542 Attn: Dr. Otto K. Heiney	1
Office of Naval Research Code 473 Arlington, VA 22217 Attn: Dr. R. Miller	10	AFRPL Code PACC Edwards AFB, CA 93523 Attn: Mr. W. C. Andrepont	1
Office of Naval Research Code 200B Arlington, VA 22217 Attn: Dr. J. Enig	1	AFRPL Code CA Edwards AFB, CA 93523 Attn: Dr. R. R. Weiss	1
Office of Naval Research Code 26D Arlington, VA 22217 Attn: Mr. D. Siegel	1	Code AFRPL MKPA Edwards AFB, CA 93523 Attn: Mr. R. Geisler	1
Office of Naval Research Western Office 1030 East Green Street Pasadena, CA 91106 Attn: Dr. T. Hall	1	Code AFRPL MKPA Edwards AFB, CA 93523 Attn: Dr. F. Roberto	1
Office of Naval Research Eastern Central Regional Office 495 Summer Street Boston, MA 02210 Attn: Dr. L. Peebles Dr. A. Wood	2	AFSC Andrews AFB, Code DLFP Washington, DC 20334 Attn: Mr. Richard Smith	1
Office of Naval Research San Francisco Area Office One Hallidie Plaza Suite 601 San Francisco, CA 94102 Attn: Dr. P. A. Miller	1	Air Force Office of Scientific Research Directorate of Chemical & Atmospheric Sciences Bolling Air Force Base Washington, DC 20332	1
Defense Technical Information Center DTIC-DDA-2 Cameron Station Alexandria, VA 22314	12	Air Force Office of Scientific Research Directorate of Aero- space Sciences Bolling Air Force Base Washington, DC 20332 Attn: Dr. L. H. Caveny	1
		Anal-Syn Lab Inc. P.O. Box 547 Paoli, PA 19301 Attn: Dr. V. J. Keenan	1

	<u>No. Copies</u>		<u>No. Copies</u>
Army Ballistic Research Labs Code DRDAR-BLP Aberdeen Proving Ground, MD 21005 Attn: Mr. L. A. Watermeier	1	Hercules Inc. Eglin AFATL/DL DL Eglin AFB, FL 32542 Attn: Dr. Ronald L. Simmons	1
Army Ballistic Research Labs ARRADCOM Code DRDAR-BLP Aberdeen Proving Ground, MD 21005 Attn: Dr. Ingo W. May	1	Hercules Inc. Magna Bacchus Works P.O. Box 98 Magna, UT 84044 Attn: Mr. E. H. DeButts	1
Army Ballistic Research Labs ARRADCOM Code DRDAR-BLT Aberdeen Proving Ground, MD 21005 Attn: Dr. Philip Howe	1	Hercules Inc. Magna Bacchus Works P.O. Box 98 Magna, UT 84044 Attn: Dr. James H. Thacher	1
Army Missile Command Code DRSME-RK Redstone Arsenal, AL 35809 Attn: Dr. R. G. Rhoades Dr. W. W. Wharton	2	HQ US Army Material Development Readiness Command Code DRCDE-DW 5011 Eisenhower Avenue Room 8N42 Alexandria, VA 22333 Attn: Mr. S. R. Matos	1
Atlantic Research Corp. 5390 Cherokee Avenue Alexandria, VA 22314 Attn: Dr. C. B. Henderson	1	Johns Hopkins University APL Chemical Propulsion Information Agency Johns Hopkins Road Laurel, MD 20810 Attn: Mr Theodore M. Gilliland	1
Ballistic Missile Defense Advanced Technology Center P.O. Box 1500 Huntsville, AL 35807 Attn: Dr. David C. Sayles	1	Lawrence Livermore Laboratory University of California Livermore, CA 94550 Attn: Dr. M. Finger	1
Ballistic Research Laboratory USA ARRADCOM DRDAR-BLP Aberdeen Proving Ground, MD 21005 Attn: Dr. A. W. Barrows	1	Lawrence Livermore Laboratory University of California Livermore, CA 94550 Attn: Dr. R. McGuire	1
Hercules Inc. Cumberland Aerospace Division Allegany Ballistics Lab P.O. Box 210 Cumberland, MD 21502 Attn: Dr. Rocco Musso	2	Lockheed Missiles and Space Co. P.O. Box 504 Sunnyvale, CA 94088 Attn: Dr. Jack Linsk Org. 83-10 Bldg. 154	1

	<u>No. Copies</u>		<u>No. Copies</u>
Lockheed Missile & Space Co. 3251 Hanover Street Palo Alto, CA 94304 Attn: Dr. H. P. Marshall Dept. 52-35	1	Naval Research Lab Code 6100 Washington, DC 20375	1
Los Alamos Scientific Lab P.O. Box 1663 Los Alamos, NM 87545 Attn: Dr. R. Rogers, WX-2	1	Naval Sea Systems Command Washington, DC 20362 Attn: Mr. G. Edwards, Code 62R3 Mr. J. Murrin, Code 62R2 Mr. W. Blaine, Code 62R	1
Los Alamos Scientific Lab P.O. Box 1663 Los Alamos, NM 87545 Attn: Dr. B. Craig, M Division	1	Naval Sea Systems Command Washington, DC 20362 Attn: Mr. R. Beauregard SEA 64E	1
Naval Air Systems Command Code 330 Washington, DC 20360 Attn: Mr. R. Heitkotter Mr. R. Brown	1	Naval Surface Weapons Center Code R11 White Oak, Silver Spring, MD 20910 Attn: Dr. H. G. Adolph	1
Naval Air Systems Command Code 310 Washington, DC 20360 Attn: Dr. H. Mueller Dr. H. Rosenwasser	1	Naval Surface Weapons Center Code R13 White Oak, Silver Spring, MD 20910 Attn: Dr. R. Bernecker	1
Naval Explosive Ordnance Disposal Facility Indian Head, MD 20640 Attn: Lionel Dickinson Code D	1	Naval Surface Weapons Center Code R10 White Oak, Silver Spring, MD 20910 Attn: Dr. S. J. Jacobs	1
Naval Ordnance Station Code 5034 Indian Head, MD 20640 Attn: Mr. S. Mitchell	1	Naval Surface Weapons Center Code R11 White Oak, Silver Spring, MD 20910 Attn: Dr. M. J. Kamlet	1
Naval Ordnance Station Code PM4 Indian Head, MD 20640 Attn: Mr. C. L. Adams	1	Naval Surface Weapons Center Code R04 White Oak, Silver Spring, MD 20910 Attn: Dr. D. J. Pastine	1
Dean of Research Naval Postgraduate School Monterey, CA 93940 Attn: Dr. William Tolles	1	Naval Surface Weapons Center Code R13 White Oak, Silver Spring, MD 20910 Attn: Dr. E. Zimet	1
Naval Research Lab Code 6510 Washington, DC 20375 Attn: Dr. J. Schnur	1		

	<u>No. Copies</u>		<u>No. Copies</u>
Naval Surface Weapons Center Code R101 Indian Head, MD 20640 Attn: Mr. G. L. MacKenzie	1	Naval Weapons Center Code 388 China Lake, CA 93555 Attn: Dr. R. Derr	1
Naval Surface Weapons Center Code R17 Indian Head, MD 20640 Attn: Dr. H. Haiss	1	Naval Weapons Center Code 388 China Lake, CA 93555 Attn: Dr. R. Reed Jr.	1
Naval Surface Weapons Center Code R11 White Oak, Silver Spring, MD 20910 Attn: Dr. K. F. Mueller	1	Naval Weapons Center Code 385 China Lake, CA 93555 Attn: Dr. A. Nielsen	1
Naval Surface Weapons Center Code R16 Indian Head, MD 20640 Attn: Dr. T. D. Austin	1	Naval Weapons Center Code 3858 China Lake, CA 93555 Attn: Mr. E. Martin	1
Naval Surface Weapons Center Code R122 White Oak, Silver Spring, MD 20910 Attn: Mr. L. Roslund	1	Naval Weapons Center China Lake, CA 93555 Attn: Mr. R. McCarten	1
Naval Surface Weapons Center Code R121 White Oak, Silver Spring, MD 20910 Attn: Mr. M. Stosz	1	Naval Weapons Support Center Code 5042 Crane, Indiana 47522 Attn: Dr. B. Douda	1
Naval Weapons Center Code 3853 China Lake, CA 93555 Attn: Dr. R. Atkins	1	Rohm and Haas Company 723-A Arcadia Circle Huntsville, Alabama 35801 Attn: Dr. H. Shuey	1
Naval Weapons Center Code 3205 China Lake, CA 93555 Attn: Dr. L. Smith	1	Strategic Systems Project Office Dept. of the Navy Room 901 Washington, DC 20376 Attn: Dr. J. F. Kincaid	1
Naval Weapons Center Code 3205 China Lake, CA 93555 Attn: Dr. C. Thelen	1	Strategic Systems Project Office Dept. of the Navy Room 1048 Washington, DC 20376 Attn: Mr. E. L. Throckmorton Mr. R. Kinert	2
Naval Weapons Center Code 385 China Lake, CA 93555 Attn: Dr. A. Amster	1	Thiokol Chemical Corp. Brigham City Wasatch Division Brigham City, UT 84302 Attn: Dr. G. Thompson	1

	<u>No. Copies</u>		<u>No. Copies</u>
USA ARRADCOM DRDAR-LCE Dover, NJ 07801 Attn: Dr. R. F. Walker	1	Georgia Institute of Technology Office of Research Administration Atlanta, Georgia 30332 Attn: Professor Edward Price	1
USA ARRADCOM DRDAR-LCE Dover, NJ 07801 Attn: Dr. N. Slagg	1	Univ. of Utah Dept. of Mech. & Industrial Engineering MEB 3008 Salt Lake City, Utah 84112 Attn: Dr. Stephen Swanson	1
U.S. Army Research Office Chemistry Division P.O. Box 12211 Research Triangle Park, NC 27709	1	Space Sciences, Inc. 135 Maple Avenue Monrovia, CA 91016 Attn: Dr. M. Farber	1
Institute of Polymer Science University of Akron Akron, OH 44325 Attn: Professor Alan N. Gent	1	Washington State University Dept. of Physics Pullman, WA 99163 Attn: Professor G.D. Duvall	1
SRI International 333 Ravenswood Avenue Menlo Park, CA 94025 Attn: Dr. Y.M. Gupta	1	Univ. of Maryland Department of Mechanical Eng. College Park, MD 20742 Attn: Professor R.W. Armstrong	1
Graduate Aeronautical Lab. California Institute of Technology Pasadena, CA 91125 Attn: Professor W.G. Knauss	1	The Catholic University of America Physics Department 520 Michigan Ave., N.E. Washington, D.C. 20017 Attn: Professor T. Litovitz	1
Pennsylvania State University Dept. of Mechanical Engineering University Park, PA 16802 Attn: Professor Kenneth Kuo	1	Sandia Laboratories Division 2513 P.O. Box 5800 Albuquerque, N.M. 87185 Attn: Dr. S. Sheffield	1
Office of Naval Research 800 N. Quincy St. Arlington, VA 22217 Attn: Dr. G. Neece Code 472	1	IBM Research Lab. K42.282 San Jose, CA 95193 Attn: Dr. Thor L. Smith	1
Thiokol Corp. Huntsville Huntsville Div. Huntsville, AL 35807 Attn: Mr. J.D. Byrd	1	California Institute of Tech. Dept. of Chemical Engineering Pasadena, CA 91125 Attn: Professor N.W. Tschoegl	1
Washington State University Dept. of Physics Pullman, WA 99163 Attn: Prof. T. Dickinson	1	Northwestern University Dept. of Civil Engineering Evanston, IL 60201 Attn: Professor J.D. Achenbach	1
University of California Dept. of Chemistry 405 Hilgard Avenue Los Angeles, CA 90024 Attn: Prof. M.F. Nicol	1	Office of Naval Research Structural Mechanics Program Arlington, VA 22217 Attn: Dr. N.L. Basdekas, Code 474	1

No. Copies

University of California 1
Berkeley, CA 94720
Attn: Prof. A.G. Evans

Texas A&M Univ. 1
Dept. of Civil Engineering
College Station, TX 77843
Attn: Professor Richard A. Schapery

SRI International 1
333 Ravenswood Ave.
Menlo Park, CA 94025
Attn: Mr. M. Hill

Los Alamos Scientific Laboratory 1
Los Alamos, NM 87545
Attn: Dr. J.M. Walsh